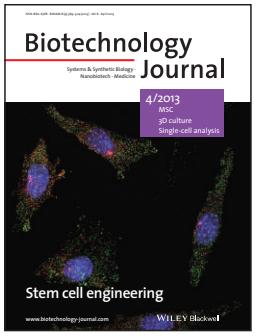

Stem cell engineering – edited by Brenda M. Ogle and Sean P. Palecek
While stem cells hold great promise for novel therapeutic strategies, our ability to harvest this potential depends on our ability to manipulate stem cells for our needs. The cover of this special issue on *Stem cell engineering* shows muscle cells undergoing differentiation, where mRNAs encoding early (green) and late (red) markers of differentiation are labeled by single-molecule fluorescence in situ hybridization. This is one method in the current repertoire of tools developed to understand the complexities of stem cells and explore their potential applications.

Biotechnology Journal – list of articles published in the April 2013 issue.

© 2013 Wiley-VCH Verlag GmbH & Co. KGaA, Weinheim

DOI 10.1002/biot.201200205 Biotechnol. J. 2013, 8, 472–484

Research Article

Mesenchymal stem cell durotaxis depends on substrate stiffness gradient strength

Ludovic G. Vincent[1], Yu Suk Choi[1], Baldomero Alonso-Latorre[2], Juan C. del Álamo[2] and Adam J. Engler[1,3]

[1] Department of Bioengineering, University of California, San Diego, La Jolla, CA, USA
[2] Department of Mechanical and Aerospace Engineering, University of California, San Diego, La Jolla, CA, USA
[3] Sanford Consortium for Regenerative Medicine, La Jolla, CA, USA

Mesenchymal stem cells (MSCs) respond to the elasticity of their environment, which varies between and within tissues. Stiffness gradients within tissues can result from pathological conditions, but also occur through normal variation, such as in muscle. MSC migration can be directed by shallow stiffness gradients before differentiating. Gradients with fine control over substrate compliance – both in range and rate of change (strength) – are needed to better understand mechanical regulation of MSC migration in normal and diseased states. We describe polyacrylamide stiffness gradient fabrication using three distinct systems, generating stiffness gradients of physiological (1 Pa/μm), pathological (10 Pa/μm), and step change (≥ 100Pa/μm) strength. All gradients spanned a range of physiologically relevant elastic moduli for soft tissues (1–12 kPa). MSCs migrated to the stiffest region on each gradient. Time-lapse microscopy revealed that migration velocity correlated directly with gradient strength. Directed migration was reduced in the presence of the contractile agonist lysophosphatidic acid (LPA) and cytoskeleton-perturbing drugs nocodazole and cytochalasin. LPA- and nocodazole-treated cells remained spread and protrusive on the substrate, while cytochalasin-treated cells did not. Nocodazole-treated cells spread in a similar manner to untreated cells, but exhibited greatly diminished traction forces. These data suggest that a functional actin cytoskeleton is required for migration whereas microtubules are required for directed migration. The data also imply that, in vivo, MSCs may preferentially accumulate in regions of high elastic modulus and make a greater contribution to tissue repairs in these locations.

Received	24 OCT 2012
Revised	13 DEC 2012
Accepted	28 Jan 2013
Accepted article online	07 FEB 2013

Supporting information available online

Keywords: Cell migration · Durotaxis · Microfluidics · Stem cell · Stiffness gradients

1 Introduction

In their native environment cells are surrounded by extracellular matrix (ECM), which transmits complex biochemical and biophysical signals [1–3]. One example of a biophysical cue is the elastic modulus of the ECM, which varies dramatically between and within tissues [4, 5] (Fig. 1A). By deforming their surroundings through cell-generated forces, cells sense this elastic modulus, often referred to as "stiffness" in the biological literature (measured in Pascals, or Pa). In the past two decades, hydrogel systems have been developed to more closely approximate native ECM stiffness [6] in order to investigate mechanically coupled cellular functions such as cell morphology, spreading, maturation, and differentiation [6–14]. The majority of work to date has focused on cell responses to substrates of uniform stiffness. However, cells in vivo may encounter dynamic environments where stiffness varies spatially, either naturally within

Correspondence: Prof. A. J. Engler, University of California, San Diego, 9500 Gilman Drive, MC 0695, La Jolla, CA 92093, USA
E-mail: aengler@ucsd.edu

Abbreviations: **APS**, ammonium persulfate; **azobis**, 2,2'-azobis(2-methylpropionamidine) dihydrochloride; **ECM**, extracellular matrix; **LPA**, lysophophatidic acid; **MSCs**, mesenchymal stem cells; **PA**, polyacrylamide; **PDMS**, polydimethylsiloxane; **TEMED**, N,N,N',N'-tetramethylethylenediamine; **UV**, ultraviolet

Color online: refer to online PDF file for figures in color.

© 2013 Wiley-VCH Verlag GmbH & Co. KGaA, Weinheim

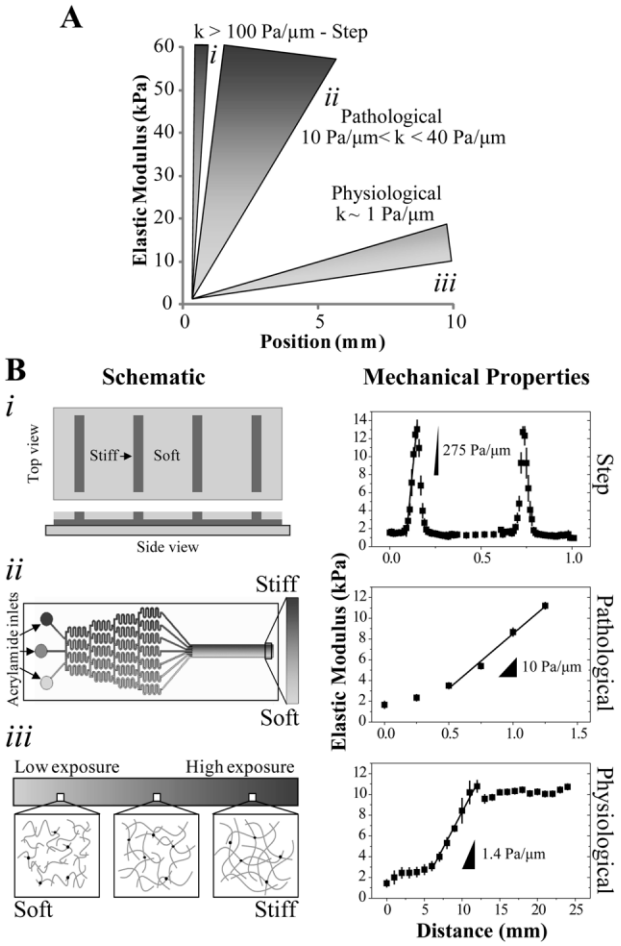

Figure 1. (**A**) Schematic representation of step (i), pathological (ii), and physiological (i) stiffness gradients. (**B**) Three separate PA systems were developed to generate mechanical gradients of varying strength and of defined range spanning ~1–10 kPa. (i) At left is a schematic of a two-stiffness hydrogel where 500 μm wide regions of soft PA alternate with ~100 μm wide strips of stiff hydrogel producing a stripped stiffness profile. At right, there is a plot of stiffness with position, indicating that the sharp transitions between soft and stiff regions create gradients of >100 Pa/μm, $n = 4$ gels. (ii) At left is a schematic of a microfluidic mixer that splits and recombines polymer solutions to generate a smooth gradient from discrete inputs. Photopolymerization of the solution in the outlet channel yields a PA hydrogel with a uniform, one-dimensional pathological stiffness gradient of 10 Pa/μm as indicated at right, $n = 3$ gels. (iii) A photomask decreasing in transparency from 100 to 30% modulates the intensity of UV that reaches the polymer solution, leading to changes in polymer chain length as illustrated at left resulting in a UV transmission gradient. This results in PA substrate with a ~1 Pa/μm mechanical gradient as shown at right, $n = 3$ gels.

tissues or as the result of a pathological condition such as the fibrotic lesions that develop after a myocardial infarct [15].

Durotaxis, the directed migration of cells up a stiffness gradient, was originally observed in fibroblasts migrating across a soft-to-stiff interface of two juxtaposed polyacrylamide hydrogels [16]. While such sharp transitions clearly illustrate this behavior, most pathological conditions create gradients that are much less steep, e.g. myocardial infarction establishes gradients ~ 8 kPa/μm [15]. Indeed, preferential migration of vascular smooth muscle cells (VSMC), but not valvular interstitial cells, has been documented on substrates ranging from ~2 to 40 kPa [17–19]. Both the range and the strength, or change in elastic modulus per unit length, of mechanical gradients describes in these studies varies. This confounds the interpretation of results, obscuring the contributions to durotaxis made by the absolute value of elastic modulus versus its rate of change across the gradient. To better understand the durotactic process, a series of gradient surfaces that encompass the same stiffness range, whilst varying in the strength of stiffness gradient, is required [20].

Mesenchymal stem cells (MSCs) are also very migratory as they must egress from the stem cell niche, migrate through tissue, and home to an injury site. Unlike terminally differentiated VSMCs, MSC also differentiate in response to mechanical stimuli, making their behavior more complex and difficult to predict. Tissue fibrosis may serve as a homing signal to guide cell migration. While biochemical signals are commonly implicated as migration cues, ECM stiffness gradients may serve as a guide to MSC migration to ensure that the right cells arrive in the right location prior to differentiation as part of the healing process [8, 21–23]. MSCs are known to undergo durotactic homing: we have previously observed MSCs undergoing directed migration even in response to shallow, physiological (1 Pa/μm) stiffness gradients [5]. The process of migration precedes MSC differentiation, making an understanding of durotaxis relevant to therapeutic application of MSC. Given the existence of stiffness variation between and within tissues, it remains to be seen whether MSC homing is driven by the stiffness range or gradient strength.

Here we sought to understand the response of MSCs to hydrogels that mimic natural tissue stiffness variations (1 Pa/μm), pathological conditions (10 Pa/μm), and tissue interfaces that present step changes in stiffness (>100 Pa/μm). We created such gradient surfaces with an identical range of stiffness of relevance to physiological soft tissue (1 – 12 kPa) [8]. To this end, we first fabricated polyacrylamide (PA) hydrogels with gradients using three separate techniques (Fig. 1B), each suited to create a specific gradient strength. Photopolymerization through a photomask yields shallow gradients due to polymer diffusion over the time scale required for polymerization [5, 17]. Microfluidic mixing chambers can create steeper gradients than photomasks, given that the input solutions and degree of mixing govern gradient strength [14, 24]. Two-step reverse cast polymerization techniques mirror previous juxtaposed polyacrylamide hydrogels [16] in such a way as to create reproducible, defined gradients. For example, Marklein and Burdick recently created 500 μm-wide stripes of alternating stiffness in hyaluronic acid

© 2013 Wiley-VCH Verlag GmbH & Co. KGaA, Weinheim

hydrogels [25], while Choi et al. [26] developed 100 and 500 μm-wide stripes of alternating stiffness in PA hydrogels. We provide the first evidence for a correlation between MSC durotactic response and gradient strength within a specified physiological range. We also suggest a potential cytoskeletal mechanism that could regulate MSC durotaxis, but not necessarily cell migration in general.

2 Materials and methods

2.1 Polyacrylamide hydrogels

Polyacrylamide (PA) hydrogels were prepared from acrylamide monomers and the crosslinker N,N'-methylene-bis-acrylamide (Fisher Scientific). PA stiffness gradients of approximately 1, 10, and 100 Pa/μm (corresponding to physiological, pathological, and step gradients, respectively) were created using three distinct systems described below. To facilitate cell attachment, human plasma fibronectin was covalently attached to the hydrogel surface. Substrates were incubated in 0.2 mM sulfo-SANPAH (Pierce) in sterile 50 mM HEPES pH 8.5, treated with UV light (wavelength 350 nm, intensity 4 mW/cm^2) for 10 min, washed three times with HEPES, and incubated with 10 μg/mL human fibronectin overnight at 37°C. Samples were stored in PBS at 4°C and UV sterilized prior to use. All chemicals were obtained from Sigma unless otherwise noted.

2.2 Fabrication of substrates with step gradients

To create hydrogels with very steep stiffness gradients, we employed a two-step polymerization scheme recently developed by Choi and co-workers [26]. First, master Si wafers were patterned with 25 mm long by 100 μm wide by 20 μm high cuboids spaced 500 μm apart using soft photolithography as described previously. SU-8 2015 was used instead of SU-8 2050, and the exposure, development, and pre- and post-bake times were adjusted according to manufacturer specification. To covalently attach substrates to glass, glass coverslips (Fisher) were cleaned of organics and oxidized by exposing both sides for 60 sec to UV/ozone (BioForce). Samples were immediately functionalized with 20 mM 3-(trimethoxysilyl)propyl methacrylate in ethanol, washed with ethanol, and dried. A Polymer solution consisting of 4% acrylamide and 0.4% bis-acrylamide 1/100 volume of 10% ammonium persulfate (APS) and 1/1000 volume of N,N,N',N'-tetramethylethylenediamine (TEMED) was pipetted in 20 μL volumes onto the wafer, covered with a methacrylated coverslip and the solution allowed to polymerize for 15 min. The hydrogel was released from the wafer and placed face down onto a 20 μL drop of polymer solution consisting of 3.2% acrylamide and 0.4% bis-acrylamide, 1/100 volume of 10% APS, and 1/1000 volume of TEMED placed on top of a dichlorodimethylsilane treated glass slide. The second solution was allowed to polymerize for 15 minutes before soaking the resulting inter-penetrating hydrogel network in DI (deionized) water. Many gradients were fabricated simultaneously from the same polymer solutions by using multiple master wafers in order to limit batch to batch variability. Two hydrogels from each polymerization batch were checked by atomic force microscopy (AFM) to verify substrate mechanical properties.

2.3 Fabrication of substrates with pathological stiffness gradients

Graded photoactivation is of insufficient resolution to achieve pathological stiffness gradients. Using the microfluidic mixing device developed by Zaari and coworkers [18] and detailed by Byfield and coworkers [27], we created gradients steep enough to mimic pathological stiffness variations [15]. Briefly, silicon wafers were cleaned with acetone, methanol, and ethanol prior to processing. Approximately 100 μm of SU-8 2050 negative photoresist (Microchem) was spin coated onto the wafer, prebaked at 65°C for 5 min and then 95°C for 20 min. The substrates were allowed to cool at room temperature before exposure to 300 mJ of 365 nm light through a transparent patterned photomask designed in AutoCad depicting the microfluidic channels (CAD/Art Services). Exposure was performed on an MA-6 mask aligner (SUSS MicroTec). A postbake was performed for 1 min at 65°C followed by 5 min at 95°C. The samples were once again allowed to cool to room temperature before being submerged for 10 min in SU-8 developer to remove the non-crosslinked regions. Samples were washed with isopropanol and dried with ultrapure nitrogen. Feature dimensions were verified using a Dektak profilometer (Veeco). Master wafers were treated overnight with (tridecafluoro-1,1,2,2-tetrahydrooctyl)-1-trichlorosilane fumes (United Chemical Technologies) to promote the subsequent polymer release. A 10:1 polydimethylsiloxane (PDMS) elastomer:curing agent solution (Sylgard 184, Dow Corning) was thoroughly mixed and degased under vacuum for 1 hour before pouring over the masters, baked at 60°C for an hour in an oven, and then released from the wafer. The resulting channels were prepped, treated for 30 sec under UV ozone along with methacrylate functionalized glass slides, and immediately reversibly bonded together. The microfluidic channels were then further processed before use by selectively wicking in a 10% solution bis(3-Triethoxysilylpropyl)disulfide (SCA 985, Struktol) in acetone into the outlet portion of the channel for 30 sec as indicated. The solution was removed from the outlet channel with vacuum and the photoinitiator solution (consisting of 10% 2,2-diethoxyacetophenone (acetophenone) in acetone) was wicked three times at 30 sec intervals into the outlet channel to remove residual SCA

© 2013 Wiley-VCH Verlag GmbH & Co. KGaA, Weinheim

985. Acetone swells the PDMS and the water insoluble hydrophobic initiator binds to the elastomer surface. Finally, photoinitiator solution was removed via vacuum. The microfluidic devices were used within the hour. Polymer solutions consisting of 10% acrylamide and either 0.05% (low) or 0.5% (high) bis-acrylamide in DI water were injected with a syringe pump (KD Scientific) at a rate of 30 µL/min into the three inlet channels. Bis-acylamide solutions were injected in the order: low-high-low. The solutions split and recombined. After reaching steady state in the outlet portion of the channel, the flow was turned off and the polymerization initiated by turning on the UV transilluminator for 6 min located directly beneath the outlet portion of the microchannel. After polymerization, the PDMS was gently removed and the resulting hydrogel, adhered to methacrylated glass 1.7 mm in width and ~2 cm in length, immediately immersed in DI water.

2.4 Fabrication of substrates with physiological stiffness gradients

A strategy for making physiological stiffness gradients was modified from Tse and Engler [28]. Photomasks decreasing in transparency from 100% to 30% were designed in Photoshop (Adobe) across different lengths. Masks were printed on transparency sheets using a 600 dpi printer. A stock polymer solution consisting of 10% acrylamide and 0.1% bis-acrylamide in DI water was prepared, stored at 4°C, and used for all experiments. Small aliquots of the polymer solution were mixed with 2,2'-azobis(2-methylpropionamidine) dihydrochloride (azobis), a photoinitiator, to a final concentratation of 0.5% w/v. A 20-µL volume of the polymer solution was sandwiched between 25 mm square methacylate- and dichlorodimethylsilane-treated slides (the former acting as an adherent base and the latter able to be released from the hydrogel after gradient formation). The glass-polymer-glass sandwich was aligned on top of the photomasks and the whole apparatus placed on the surface of a benchtop UV transilluminator equipped with 1 mW/cm^2 tubes producing light of wavelength 305 nm. A cutout was placed around and below the photomask to prevent stray light from influencing polymerization. After polymerization for 6 min, the substrate was removed and immediately immersed in water to remove unreacted species. Samples were created from the same polymer solution mixture, and two hydrogels from each polymerization batch were checked by atomic force microscopy to verify consistent substrate mechanical properties.

2.5 Material stiffness and surface topography

Force-mode AFM was performed to determine the mechanical properties of the various hydrogels. Samples were mounted on glass slides using vacuum grease and then on the AFM stage (3DBio; Asylum Research). Samples were indented 300 nm using gold-coated, pyramid-shape SiN cantilevers (TR400PB; Olympus) with ~25 pN/nm nominal spring constants as determined from indentations on a silicon surface and thermal calibration. Measurements were taken every 500–1000 µm, 250–500 µm, and 10–50 µm for stiffness gradients of 1, 10, and >100 Pa/µm, respectively. Force curves were analyzed in Igor (WaveMetrics) using a linearized Hertz model to determine the Young's modulus [29]. For 100 Pa/µm gradients, the soft-stiff transition topography and modulus were obtained with 90 × 90 µm force maps.

2.6 Cell culture

Human MSCs (Lonza Walkersville) were cultured in low glucose Dulbecco's modified eagle medium (DMEM) supplemented with 10% fetal bovine serum and 1% penicillin /streptomycin 100× solution (Gibco). For culture maintenance, media was changed every three days and cells passaged before reaching confluence to maintain multipotency. Stem cells between passages 4–8 were used for all experiments. Cells were seeded at 5×10^3 to 2.5×10^4 cells/mL and media changed every 2–3 days. For inhibitor studies, lysophosphatidic acid (LPA, Enzo Life Scienes), nocodazole and cytochalasin D (Sigma) were used at a final concentration of 20 µM, 0.5 µM, and 2 µM, respectively. Inhibitors were dissolved in dimethyl sulfoxide (DMSO), stored at –20°C and the final concentration of DMSO in the media did not exceed 0.1% v/v.

2.7 Immunofluorescent staining and imaging

Cells were fixed with 10% formalin for 15 min at room temperature. Actin cytoskeleton was stained with 1:500 rhodamine phalloidin (Invitrogen, Carlsbad, CA) in 1% bovine serum albumin and a wash buffer (1 mM $MgCl_2$ in phosphate buffered saline) for 30 min at 37°C. After rinsing thrice with wash buffer, nuclei were stained with 3.2 µM Hoechst 33342 for 10 min at room temperature. For surface protein visualization, fibronectin-coated hydrogels were incubated with 1:500 R457 [30] rabbit polyclonal anti-rat antiserum against the amino-terminal 70 kDa fragment of fibronectin in staining solution for 30 min at 37°C, washed thrice with buffer, and then incubated with 1:500 AlexaFluor 488-conjugated secondary antibody (1:500; Invitrogen) for 30 min at 37°C. All samples were washed with DI water and mounted using Fluoromount-G (SouthernBiotech). Samples were imaged by a CARV II confocal (BD Biosciences) Nikon Eclipse Ti microscope equipped with a TE2000-U motorized, programmable stage using a Cool-Snap HQ camera (Photometrics) and controlled by Metamorph 7.6 (Molecular Devices). For time-lapse measurements, cells were placed inside a temperature, CO_2, and humidity controlled LiveCell chamber (Pathology Devices) and custom Metamorph journals acquired, reconstructed, and processed multi-positional

© 2013 Wiley-VCH Verlag GmbH & Co. KGaA, Weinheim

scan slides images. Post-processing was performed in Methamorph 7.6 and ImageJ (NIH).

2.8 Traction force microscopy (TFM)

TFM was performed as described elsewhere using in-house Matlab (Mathworks) routines [31]. 2% v/v of 0.5 μm diameter Fluoresbrite YG Microspheres (Polysciences, Inc) were added to the polymer solutions prior to gelation and the positions of the beads acquired over time using fluorescent and brightfield time-lapse microscopy. After cell trypsinization, bead positions were acquired again and displacement maps were generated using image correlation algorithms similar to particle image velocimetry [32]. Traction stress maps were determined from the measured displacement maps by solving the equation of elastic equilibrium for the substrate. The hydrogel's spatially-varying mechanical properties were considered by performing a perturbation expansion of the solution in terms of the stiffness gradient [33]. Samples were again imaged by a CARV II confocal (BD Biosciences) Nikon Eclipse Ti microscope equipped with a TE2000-U motorized, programmable stage using a Cool-Snap HQ camera (Photometrics) and controlled by Metamorph 7.6 (Molecular Devices). Cell velocities were computed with ImageJ and only migration along the gradient direction was measured. The error in migration velocities measurements due to the spatial resolution of the images is on the order of 1 μm/hr.

2.9 Statistical analyses

All data are expressed as mean ± standard deviation of experiments unless otherwise noted. Non-parametric Wilcoxon rank-sum tests were used to perform all statistical analysis. Differences were considered significant when $p<0.005$ and indicated for all comparisons. All experiments were performed in triplicate unless otherwise noted, and in such cases, the number of cells used in the measurement has been stated.

3 Results

3.1 Fabrication of hydrogels with stiffness gradients

To generate physiological, pathological, and step stiffness gradients of defined range corresponding to approximately 1 Pa/μm, 10 Pa/μm, and 100 Pa/μm respectively (Fig. 1A), we utilized three distinct systems (Fig. 1B). Since our goal was to investigate the migration behavior of human MSCs solely based on gradient strength, system parameters were chosen such that the stiffness range was identical across all systems, spanning 1 to 12 kPa.

For step gradients, a two-step polymerization mechanism was used, resulting in mechanically-patterned matrix. The stiff, bottom hydrogel was first polymerized on top of a micropatterned Si wafer; a second polymer solution was subsequently added on top of the first where it could selectively polymerize into the 'fingers' of the first layer, making them even stiffer, or it could be retained in grooves where it formed a softer hydrogel (Fig. 1B*i*) [26]. To highlight this, top and bottom hydrogel composition was set to be relatively similar – 3.2% vs. 4.0% acrylamide, respectively– but the bottom hydrogel's stiffness after a second polymerization was roughly 13 kPa (Fig. 1B*i*), four times the expected value when polymerized as a thin film (Supporting information, Fig. S1). Changing the bottom hydrogel composition by increasing the acrylamide percentage led to stiffer bottom hydrogels (Supporting information, Fig. S1A), but also magnified the stiffening effect that occurred during the second polymerization step. For instance, increasing the bottom hydrogel's stiffness to 7.4 kPa by using a 6% acrylamide solution (Supporting information, Fig. S1A) resulted in a mechanically-patterned matrix whose stiff regions consistently exceeded 100 kPa (Supporting information, Fig. S1B). The transition distance from soft to stiff stripes occurred over approximately 40 μm, effectively creating a stiffness gradient of 275 Pa/μm whose range spans an order of magnitude, i.e. 1 to 13 kPa (Fig. 1B*i*). It is important to note that these hydrogels have a continuous top layer made with a high concentration of crosslinker-containing solution, i.e. 0.4% bis-acrylamide, which minimizes topographical differences [26].

For pathological stiffness gradients, a microfluidic mixing device made out of polydimethylsiloxane (PDMS) was used to generate hydrogels with varying mechanical properties [18, 27]. Solutions with different concentrations of bis-acrylamide crosslinker but similar acrylamide concentrations are injected into the inlets of the microchannel device (Fig. 1B*ii*) after the outlets had been functionalized with SCA 985 to facilitate the later release of the hydrogel from the mold, and the photoinitiator acetophenone to confine polymerization to the outlet channel (Fig. 2A). As the solutions reach the branch points, they split and recombine, in the process mixing and generating a gradient of crosslinker in the outlet portion of the channel (Fig. 2B and 2C). Photopolymerization of the solution produced a hydrogel with a defined stiffness gradient up to 10 Pa/μm (Fig. 1B*ii*). Modulating crosslinker concentration in microchannel inlets changed the stiffness profile of the resulting hydrogel including the gradient range and magnitude (data not shown).

Several design changes from previous PDMS microfluidic mixing devices [18, 24, 34] incorporated into our design to ensure a consistent gradient with minimal swelling, limited topographical features, and a range of approximately 1 to 12 kPa. In attempts to achieve the target stiffness range by optimizing photoactivation for previously published methods, polymer solutions that normally yield 40 kPa substrates using the APS/TEMED ini-

© 2013 Wiley-VCH Verlag GmbH & Co. KGaA, Weinheim

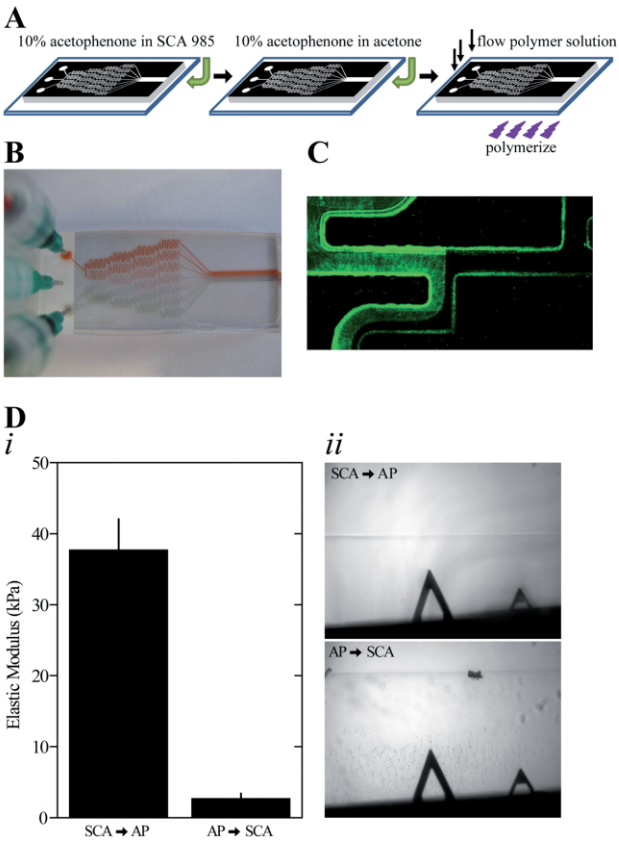

Figure 2. (**A**) Schematic of the microfluidic gradient generator preparation process. (**B**) Image of the microfluidic gradient generator with inlets containing red, green, or no food coloring in water to visualize mixing in the channel. (**C**) Magnified fluorescent image of active flow in the microfluidic gradient generator at a branch point. The left inlet contains EosinY. (**D**) A solution was polymerized in the outlet of the gradient generator with acetophenone dissolved in SCA 985 or acetophenone dissolved in acetone and SCA 985 subsequently added. (i) Hydrogel stiffness is shown for the indicated order of adding acetophenone and SCA 985 to the gradient generator output channel. Error bars depict standard deviation. Measurements in triplicate were made at 6 distinct positions, $n = 3$ gels. (ii) Phase contrast images are shown of the hydrogel edge when either SCA 985 or acetophenone was added first in the preparation process.

tiator system yielded hydrogels with elastic modulus of less than 2 kPa (Supporting information, Fig. S2A) [18]. Moreover, a number of of polymer concentrations and photoinitiators tested, including irgacure 2959 and azobis, could not create a gradient when polymerized inside the PDMS microchannel. Polymerization through fused quartz, which has superior UV transmission properties to glass [35], did not significantly increase gradient slope in the PDMS device (Supporting information, Fig. S2B). Instead, acetophenone was adsorbed onto the PDMS surface of the outlet channel to deliver it locally to the polymer solution [36]. Photopolymerization of static hydrogels inside the outlet portion produced substrates with the same mechanical properties as thin films (Fig. 2D*i*). In contrast, when acetophenone was flowed through the outer channel prior to coating of the channel PDMS surface with SCA 985, softer hydrogels with numerous surface defects that may interfere with cell adhesion resulted (Fig. 2D)].

Photomasks allow the spatial control of the amount of UV light reaching the PA solution, permitting modulation of photopolymerization kinetics (Fig. 1B*iii*). To achieve physiological gradients, we adapted a photoactivated polymerization procedure used by Tse and Engler (Fig. 3A) [5]. Substituting in a linear photomask to more easily change gradient distance and using the more water-soluble initiator azobis, we were able to modulate gradient strength ten -fold, e.g. from 0.38 to 3.46 Pa/μm, even for gradient hydrogels with narrow stiffness ranges, i.e. 1–5 kPa (Fig. 3B). For any given photomask, changing the polymer solution concentration, and thus the gradient hydrogel's stiffness range, also changes the gradient strength from ~0.4 to 4 Pa/μm (Fig. 3C). Tailoring this system to our specifications, we are able to span the 1 to 12 kPa range at a gradient strength of ~1 Pa/μm (Fig. 1B*iii*) using a 12 mm opacity gradient photomask and a 10% acrylamide/0.1% bis-acrylamide solution.

3.2 Directed cell migration on stiffness gradients

Prior to cell adhesion, each PA hydrogel was functionalized with fibronectin to promote cell attachment to an otherwise inert substrate. Since gradients were produced using more than one method and varied in stiffness strength, it was important to verify that the protein coating was consistent across individual gels, i.e. independent of substrate stiffness. Confocal cross-sections of fluorescently-labeled fibronectin indicated that there were no qualitative differences in protein attachment as a function of fabrication method, gradient strength, or absolute stiffness (Fig. 4). Thus subsequent cell behavior differences should not be the result of spatial changes in surface ligand density.

MSCs attached and spread independent of gradient strength or stiffness within hours of seeding, and after 3 days, cells migrated to stiffer portions of the substrates. Migration was most evident on step and pathological gradients (Fig. 5A). It is important to note that MSCs also migrate in response to physiological stiffness gradients, although this is less evident in short-term experiments [28]. To verify cell migration and to eliminate the possibility that the spatial differences in cell density were due to preferential proliferation on stiffer regions [13], durotactic migration velocity, i.e. migration in the direction of the gradient, was measured from time-lapse video microscopy. The distribution of instantaneous migration speeds was broad for cells on physiological and pathological gradients (Fig. 5B), yet the population average indicated a net biased migration in the direction of the gradient at a rate of 3.0 ± 0.7 and 6.2 ± 0.6 μm/hr for physiological and

© 2013 Wiley-VCH Verlag GmbH & Co. KGaA, Weinheim

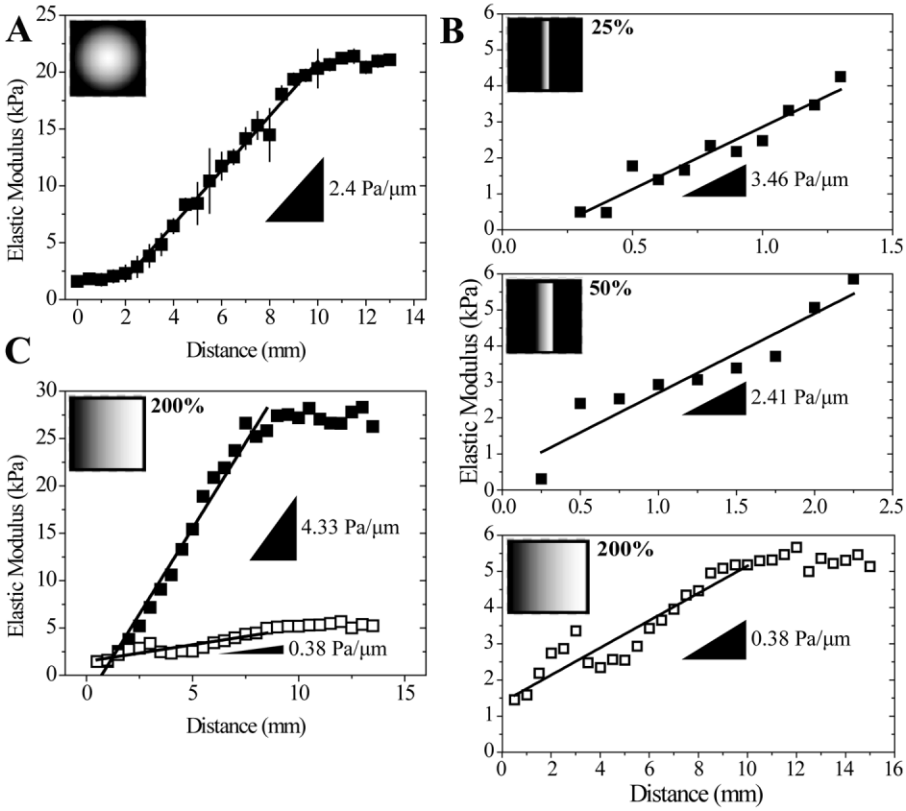

Figure 3. (**A**) Gradients generated using a radially symmetric mask and a solution containing 10% acrylamide, 0.3% bis-acrylamide, and 0.5% irgacure as the initiator ($n = 4$ gels). (**B**) Gradients produced with the same polymer solution (10% acrylamide, 0.1% bis-acrylamide) but using photomasks where the opacity gradient was scaled to 25%, 50%, or 200% of the distance used in Fig. 1Bii, $n = 1$. (**C**) Two different gradients made with the same photomask but different polymer solutions. Closed squares: 10% acrylamide and 0.3% bis-acrylamide, open squares: 10% acrylamide, 0.1% bis-acrylamide, $n = 1$. Insets of **(A)–(C):** Photomask images used for gradient fabrication with indicated photomask gradient distance relative to the photomask in Fig. 1Bii.

pathological gradients, respectively (Fig. 5C). Cells on step gradients migrated at 18.0 ± 0.7 μm/hr, more than six-fold faster than on other gradient strengths. It should be noted that cell tracks with negative velocities were not observed for cells migrating up step gradients. These data imply that biased migration velocity scales directly with gradient strength over two orders of magnitude, i.e. 1 to >275 Pa/μm (Fig. 5C inset).

3.3 Regulating directed cell migration

Since cell migration results from the coordination of cytoskeleton assembly and disassembly in both space and time, we sought to understand which elements were crucial for durotaxis. To do this, we treated MSC with three molecules: lysophosphatidic acid (LPA), a contractile agonist, and cytoskeleton-perturbing drugs nocodazole and cytochalasin D. Cells treated with nocodazole cannot form stable microtubules, whilst cytochalsain D prevents actin polymerization. Cells treated with LPAand nocodazole-treated cells exhibited a similar footprint, more spread than untreated controls. thatIn contrast cytochalasin D-treated spread less than untreated cells (Fig. 6A). Untreated cells on gradient substrates did not differ in spread area compared to cells on static matrices (3570 ± 340 μm^2 vs. 3400 ± 260 μm^2). After three days in culture, untreated cells polarized their actin cytoskeleton in the direction of a pathological gradient, e.g. 8.7 ± 1.9 Pa/μm, whereas

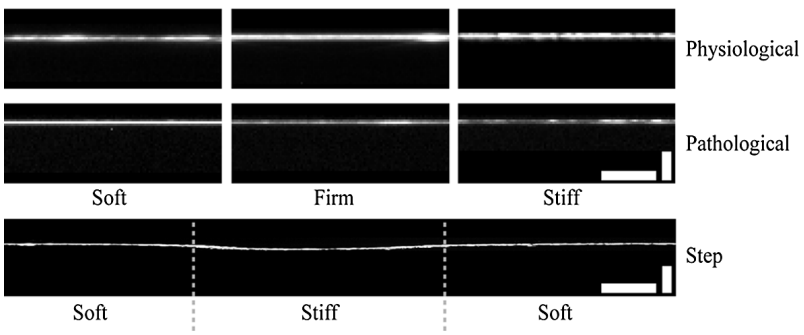

Figure 4. Representative confocal cross-sections of each hydrogel system with fluorescently-labeled human plasma fibronectin. Each physiological gradient and pathological gradient image was averaged over 13 overlapped fluorescent cross-sections and repeated at least twice. Scale bars are 25 μm (horizontal) and 5 μm (vertical) for the physiological and pathological gradients and 25 μm (horizontal) and 20 μm (vertical) for step gradient.

© 2013 Wiley-VCH Verlag GmbH & Co. KGaA, Weinheim

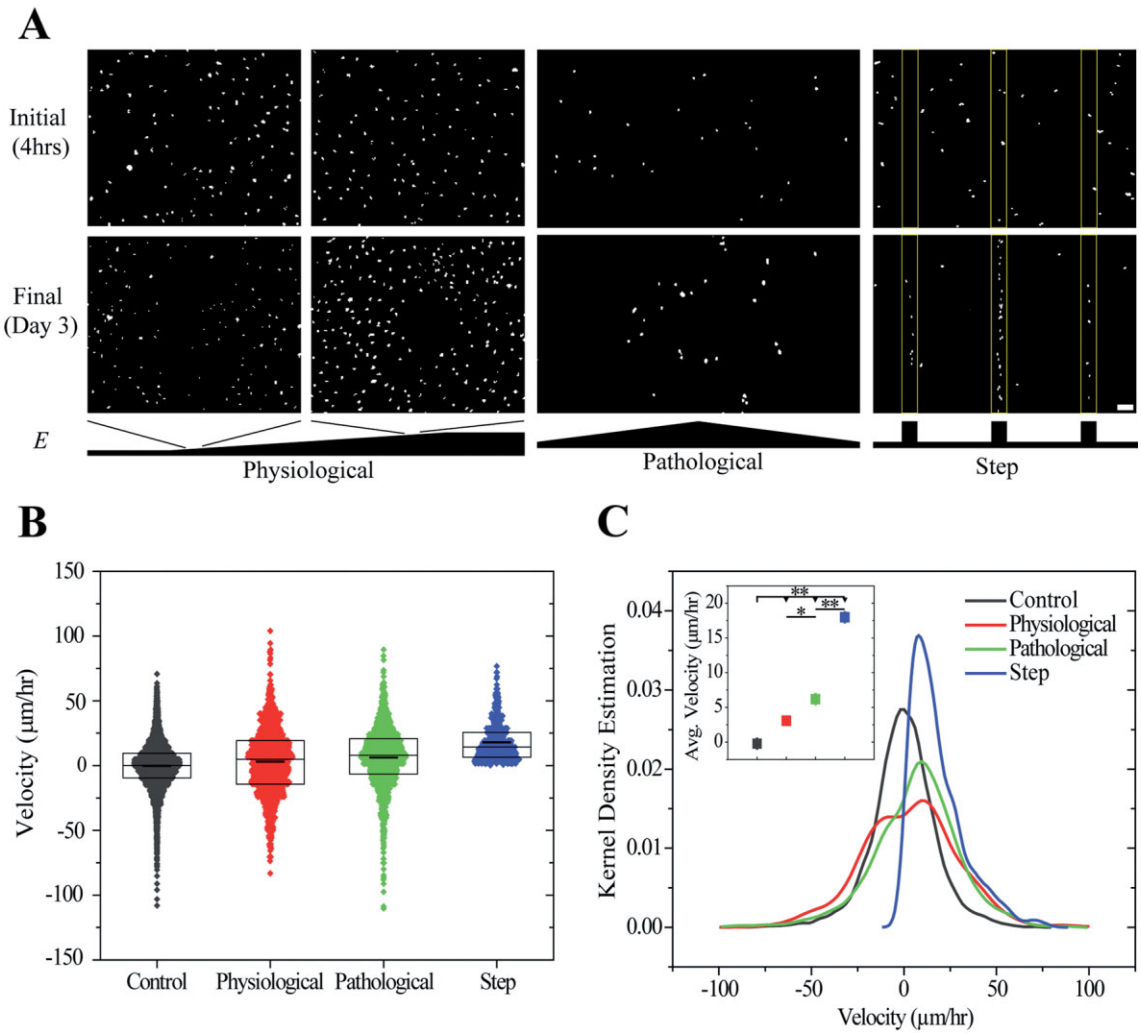

Figure 5. (**A**) Thresholded images of Hoechst-stained MSCs on physiological (1.4 Pa/μm), pathological (10 Pa/μm), and step gradients (275 Pa/μm) 4 hours and 3 days after plating. Scale bar is 100 μm. (**B**) Velocities of migrating MSCs in the direction of the gradient determined from tracking live cells using time-lapse microscopy on physiological, pathological, and step gradients. Boxes indicate median, 25th, and 75th percentile and the thicker line indicates the average. (**C**) Kernel density estimation of cell velocities on the three gradient systems and average ± standard error of cell migration velocity for each system (inset). **p*-value < 10^{-2}, **p-value <10^{-5}. For step gradient, n=450 independent velocities. For physiological and pathological gradients, *n* > 1300 independent velocities. Data were obtained from 3 biological replicates.

LPA-treated cells were randomly polarized and nocodazole- and cytochalasin D-treated cells maintained a rounded morphology (did not polarize) (Fig. 6B). All treatments impaired durotaxis significantly (Fig. 6C), but while cytochalasin D- and nocodazole-treated MSCs remained largely stationary, LPA-treated MSCs remained spread, protrusive and migrated randomly (Supporting information, videos 1–4). Together, these data suggest that a stable actin cytoskeleton under appropriate tension is essential for MSC spreading. Microtubule formation in particular is required for MSC polarization to initiate directed migration.

To determine if the directed migration of MSCs was due to contractile differences as a result of cytoskeletal changes caused by drug treatments, we performed TFM on durotaxing MSCs plated on these gradients. Since MSCs were plated onto gradients, TFM software used to calculate traction stresses was specifically modified to adjust for a spatial stiffness gradient. These changes are detailed elsewhere [33]. Over time, deformations on the stiffer, right side of the image for an untreated cell increased while cell deformations on the softer side decreased, resulting in MSC directed migration. In contrast, nocodazole-treated cells only slightly deformed the hydrogel despite changing morphology (Fig. 6D). Converting displacements to traction forces and taking into account the graded mechanics of the hydrogel, untreated migrating MSCs are also better at forming force-generat-

© 2013 Wiley-VCH Verlag GmbH & Co. KGaA, Weinheim

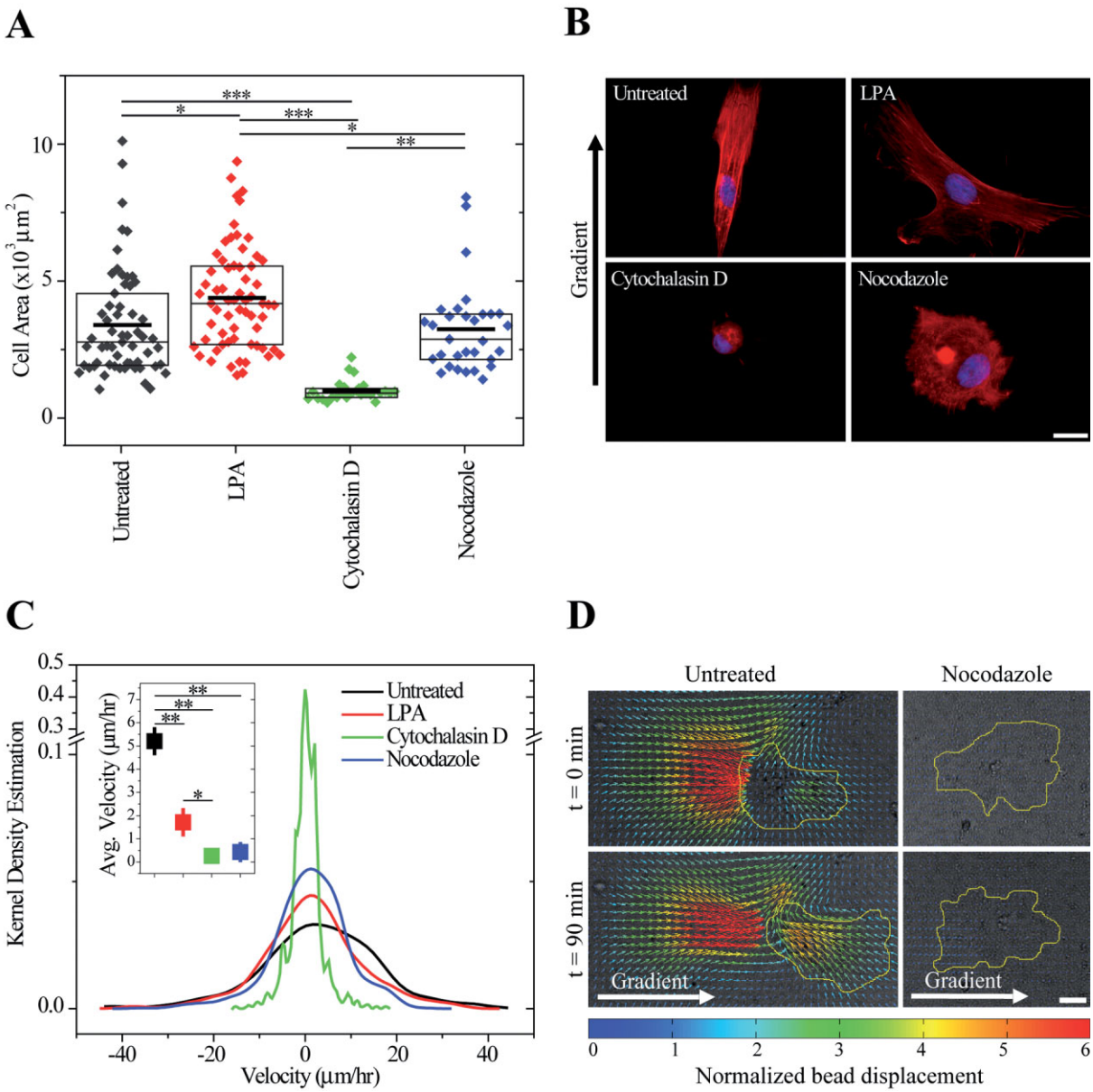

Figure 6. (**A**) Spread area of MSCs on gradients either untreated (gray) or treated with lysophosphatidic acid (red), cytochalasin D (green), or nocodazole (blue) after 3 days. Boxes indicate median, 25th, and 75th percentile and the thicker line indicates the average. $n > 27$ cells for each condition. (**B**) Nuclei (blue) and actin (red) of MSCs stained after 3 days in culture with inhibitors. Scale bar is 20 µm. (**C**) Migration of untreated and inhibitor treated MSCs on hydrogel with a pathological gradient of 8.7 ± 1.9 Pa/µm and range of 1 to 12 kPa. Inset depicts average ± standard error of cell migration velocity for each condition. For each condition, $n > 460$ independent velocities. Data were obtained from 2 biological replicates. (**D**) Displacement maps of fluorescent particles embedded in the hydrogel obtained using particle image velocimetry for untreated and nocodazole-treated cells. Brightfield images and cells contours in yellow are overlaid with the displacement maps. Gradient is from left to right. Scale bar is 30 µm. *p-value < 10^{-2}, **p-value <10^{-5}.

ing protrusions than nocodazole-treated cells (Supporting information, videos 5 and 6). These data indicate that stable microtubules are crucial to generate directed traction forces that encourage durotaxis but not essential for some modes of spreading.

4 Discussion

To study durotaxis over a range of gradient strengths (1 to >100 Pa/µm) with a consistent defined stiffness range (1 to 12 kPa) we developed three individual hydrogel systems, each of which was optimally suited for particular gradient strengths. Within that context, it is also critical to appreciate basic mechanistic reasons behind cell

© 2013 Wiley-VCH Verlag GmbH & Co. KGaA, Weinheim

migration. Below, we place the implementation of the elastic gradient systems described and the subsequent analysis of MSC behavior within a broader context.

4.1 Challenges of fabricating reproducible gradient hydrogel systems of varying gradient strength and stiffness range

A variety of methods have been used to achieve spatial stiffness gradients, but each has a limited range of stiffness and gradient strength. Each method also requires standardizing methods to ensure that the gradient is reproducible and that there are no other mitigating factors that could unduly influence cell behavior. We have provided an overview of the fabrication of three stiffness gradient hydrogel systems, noting their range and strength. Here we compare these to similar systems used previously to fabricate stiffness gradients.

For photolithographically patterned gradients, modulating light intensity to change radical polymerization kinetics has previously been attained using photomasks [5, 17] or sliding masks [37, 38] to vary hydrogel UV exposure time. This technique is well suited for the generation of physiological to pathological strength gradients. We show its versatility in precisely controlling both the range and strength of gradients between 0.4 and 8.7 Pa/μm and 1 to 12 kPa. In this work, azobis was used as the photoinitiator, due to its increased solubility in aqueous solutions and activation using long wave UV. Previous work used irgacure to initiate acrylamide polymerization [5]. Silica glass does not transmit below 300 nm, and since irgacure's peak absorption occurs at 276 nm, its reaction is always suboptimal in this setting [35, 39]. Light diffraction and lateral diffusion of radicals also limit the resolution resolution of gradients created using photomasks. However, high resolution photomasks have been used to pattern binary changes in hydrogel surface compliance at the micron lengthscale [25]. Microfluidic channels more tightly constrain hydrogel dimensions and provide superior control over stiffness at the micron length scale, resulting in higher gradient resolution and the capability to increase gradient strength. In microfluidic fabricated hydrogel gradients, stiffness is modulated by changing crosslinker concentration along the width of the hydrogel, instead of modulating initiator activation [18, 24, 27]. Changing input solutions is simple, and allows for systematic spatial control over the mechanics in the outlet channel. However, PDMS, the common material used to form microfluidic devices,is porous and allows molecular oxygen to diffuse through the surface, which reacts with radicals generated by the photoinitiator, effectively terminating the polymerization reaction [40, 41]. The effect has been minimal in rapidly polymerizing systems such as poly(ethylene glycol) and may even be advantageous as the non-polymerized layer at the interface of the hydrogel and PDMS serves as a lubricating layer and promotes hydrogel release [24, 41]. In our hands, for polyacrylamide hydrogels formed using a radical-based polymerization that takes place over several minutes, oxygen radical scavengers in PDMS prevented the synthesis of hydrogels above 2 kPa. A number of water-soluble initiators, initiator concentrations, and UV treatments were unsuccessfully trialed to overcome this issue, despite studies reporting otherwise [18, 20]. Absorbing hydrophobic acetophenone to the surface of PDMS allows for the polymerization of stiff PA hydrogels [27, 36], presumably because the initiator-generated radicals saturate at the PDMS surface, limiting the amount available to diffuse into the polymer solution. However, PA polymerization with this method lacks the lubricating layer, and thus the PA grafts into the PDMS [27]. This prevents release and may cause the substrate to rip. SCA 985 covalently bound to the PDMS surface maintains the lubricating layer. By coating PDMS using SCA 985 prior to absorbing acetophenone, stiff hydrogels were released from the PDMS mold without damaging the substrate surface.

There are also several challenges associated with creating step stiffness gradients from mechanically-patterned substrates. For example, the original method of polymerizing adjacent droplets of distinct acrylamide concentrations [16] forms a gradient from uncontrolled mixing, and, while microfluidic gradients are well controlled, they often cannot achieve the steepest gradients required, i.e. >100 Pa/μm [18, 24, 27]. Controlling the transition from soft to stiff was recently described by using a 2-step polymerization method to make mechanically-patterned hydrogels [25, 26]. Here, by increasing the soft region width, we allowed cells to spread and randomly migrate before encountering the gradient near the interface and undergoing directed migration to the stiffer region. Though we used this system to understand migration up an exceedingly steep gradient, this platform has also been used to study the relationship between cell alignment and function [26]. There are technical challenges specific to the fabrication of step gradients worth noting: differential swelling between layers in microfabricated hydrogels has been reported and could introduce contract guidance cues similar to topographical patterns. By using substrates with high crosslinker content however [42], polymer chains are restricted from sliding across each other, dramatically reducing differential swelling between layers to less than 2 μm. Roughness changes between stripes on the hydrogel are also minimized to less than 200 nm [26]. A second challenge with bi-layer hydrogel fabrication is that polymer depletion effects in the soft stripes formed by the second layer's polymerization also confound the prediction of layer stiffness. Small changes in bottom hydrogel stiffness dramatically change the final stiffness after the second acrylamide solution is polymerized. Stiffness measurements of the top hydrogel in the step gradient significantly deviated from those of the same hydrogel as a monolayer [5]. Materials that do

© 2013 Wiley-VCH Verlag GmbH & Co. KGaA, Weinheim

not undergo such mixing may form more predictable layered materials (for example, PDMS) [43].

Despite these challenges, it should be noted that, across all three systems, protein coating appeared uniform and initial cell adhesion was similar independent of polymer concentration and crosslink density.

4.2 The origins of durotaxis

Cells plated on the gradient systems migrated to the stiffer end of the hydrogels at different speeds, indicating that MSC durotaxis velocity depends on gradient strength, as previously suggested with other cell types [20] but demonstrated over a wider range of gradients here. It is important to note that the migration velocities reported here were obtained over the same physiological stiffness range of 1 to 12 kPa, indicating that gradient strength and not absolute stiffness drove directed MSC migration on gradient substrates. It was evident that MSCs did not respond to the gradient in the same manner. In step gradients for the mechanically-patterned hydrogels; MSCs that approached the interface between low and high stiffness migrated faster than indicated by the time-averaged measurement recorded. Thus migration speed of 18 μm/hr given could be an underestimation. Despite that consideration, it is clear that durotactic speed increases with gradient strength, but the relationship between migration rate and gradient strength is not linear. In addition to speed, cell traction forces enable MSCs to detect stiffness gradients and then migrate, but as of yet, this mechanisms behind this process remains unclear. Neutrophils, which undergo amoeboid-like migration, form rearward contractile centers, which subsequently squeeze the cell forward in the direction of a chemotactic gradient [44, 45]. This process, though different from the multi-step mesenchymal migration of MSCs [46], also requires myosin II [47]. Interestingly, MSC traction distribution in cells migrating up stiffness gradients seemingly mirrors the rearward contractile stresses observed in neutrophils. One plausible explanation may be that cells perceive the elastic modulus of their environment by sensing the strain they can impart on their matrix [48].

Reporter bead displacements were observed to be highest at the rear of cells migrating up stiffness gradients, suggesting that this is where strain sensors are most active in transmitting information on substrate compliance to the cell. A variety of strain sensors have been proposed [49–51] and likely require some minimum level of signaling to encourage cell behaviors such as spreading and migration [52, 53].The sensors required for this process, and thus their signaling capabilities, are likely connected to the cell cytoskeleton, since altering the cell's ability to assemble a stable cytoskeleton significantly reduced MSC migration. However, these observations did not necessarily correlate with changes in cell spread area. The loss of microtubule architecture inhibited cell polarity, with the cells remaining spread yet non-migratory. Similar to a previous report on nocodazole-treated fibroblasts [54], MSCs appear to require assembled microtubules to transmit forces to their surrounding environment, but an actin cytoskeleton is necessary to adopt a spread morphology. Interestingly, cells treated with the multifunctional phospholipid messenger LPA, which promotes activation of the Rho and Ras GTP-ases [55] and thus increases the tension able to be exerted by a cell [56], did not undergo directed migration despite their heightened ability to 'feel' matrix stiffness [57]. LPA signaling is thought to contribute to cancer initiation, progression, and metastasis [58], though our results also suggest the inhibition of durotaxis. This observation is particularly relevant to undertstanding the mechanisms responsible for durotaxis, since the migration of untreated cells up the gradient relies on their ability to deform the matrix and generate traction stresses on the order of a few hundred Pascals.

5 Conclusions

Together these data imply that durotaxis mechanism(s) are force dependent, require an assembled microtubule network, and also require precise coordination of contractility in time and space since both increased and decreased cell contractility abolished directed migration. More importantly, through the development of these three platforms, it was possible to fabricate gradients of the necessary range and strength to answer these questions.

The authors would like to thank Drs. Somyot Chirasatitsin and Alexander Fuhrmann for technical assistance with atomic force microscopy and quantification of cell spread areas, respectively. This work was supported by grants from the NIH (DP02OD006460 to A.J.E., and 1R01GM084227 to J.C.A), the Human Frontiers Science Foundation (RGY0064/2010 to A.J.E.), Graduate Research Fellowship from the National Science Foundation (to L.G.V), and Achievement Rewards for College Scientists Fellowship (to L.G.V).

The authors declare no conflict of interest.

6 References

[1] Hynes, R. O., The extracellular matrix: not just pretty fibrils. *Science* 2009, *326*, 1216–1219.
[2] Badylak, S. F., Regenerative medicine and developmental biology: the role of the extracellular matrix. *Anat. Rec. B New. Anat.* 2005, *287*, 36–41.
[3] Hay, E. D., Extracellular matrix. *J. Cell. Biol.* 1981, *91*, 205s–223s.

© 2013 Wiley-VCH Verlag GmbH & Co. KGaA, Weinheim

[4] Vincent, L., Engler, A. J., 5.504 – Effect of substrate modulus on cell function and differentiation, in: Paul, D. (Ed.), *Comprehensive Biomaterials*, Elsevier, Oxford 2011, pp. 51–63.
[5] Tse, J. R., Engler, A. J., Stiffness gradients mimicking in vivo tissue variation regulate mesenchymal stem cell fate. *PLoS One* 2011, *6*, e15978.
[6] Discher, D. E., Mooney, D. J., Zandstra, P. W., Growth factors, matrices, and forces combine and control stem cells. *Science* 2009, *324*, 1673–1677.
[7] Saha, K., Keung, A. J., Irwin, E. F., Li, Y. et al., Substrate modulus directs neural stem cell behavior. *Biophys. J.* 2008, *95*, 4426–4438.
[8] Engler, A. J., Sen, S., Sweeney, H. L., Discher, D. E., Matrix elasticity directs stem cell lineage specification. *Cell* 2006, *126*, 677–689.
[9] Huebsch, N., Arany, P. R., Mao, A. S., Shvartsman, D. et al., Harnessing traction-mediated manipulation of the cell/matrix interface to control stem-cell fate. *Nat. Mater.* 2010, *9*, 518–526.
[10] Discher, D. E., Janmey, P., Wang, Y. L., Tissue cells feel and respond to the stiffness of their substrate. *Science* 2005, *310*, 1139–1143.
[11] Flanagan, L. A., Ju, Y. E., Marg, B., Osterfield, M., Janmey, P. A., Neurite branching on deformable substrates. *Neuroreport* 2002, *13*, 2411–2415.
[12] Wozniak, M. A., Chen, C. S., Mechanotransduction in development: a growing role for contractility. *Nat. Rev. Mol. Cell Biol.* 2009, *10*, 34–43.
[13] Pelham, R. J., Jr., Wang, Y., Cell locomotion and focal adhesions are regulated by substrate flexibility. *Proc. Natl. Acad. Sci. USA* 1997, *94*, 13661–13665.
[14] Wong, J. Y., Leach, J. B., Brown, X. Q., Balance of chemistry, topography, and mechanics at the cell–biomaterial interface: Issues and challenges for assessing the role of substrate mechanics on cell response. *Surf. Sci.* 2004, *570*, 119–133.
[15] Berry, M. F., Engler, A. J., Woo, Y. J., Pirolli, T. J. et al., Mesenchymal stem cell injection after myocardial infarction improves myocardial compliance. *Am. J. Physiol. Heart Circ. Physiol.* 2006, *290*, H2196–2203.
[16] Lo, C. M., Wang, H. B., Dembo, M., Wang, Y. L., Cell movement is guided by the rigidity of the substrate. *Biophys. J.* 2000, *79*, 144–152.
[17] Wong, J. Y., Velasco, A., Rajagopalan, P., Pham, Q., Directed movement of vascular smooth muscle cells on gradient-compliant hydrogels. *Langmuir* 2003, *19*, 1908–1913.
[18] Zaari, N., Rajagopalan, P., Kim, S. K., Engler, A. J., Wong, J. Y., Photopolymerization in microfluidic gradient generators: microscale control of substrate compliance to manipulate cell response. *Adv. Mater.* 2004, *16*, 2133–2137.
[19] Kloxin, A. M., Benton, J. A., Anseth, K. S., In situ elasticity modulation with dynamic substrates to direct cell phenotype. *Biomaterials* 2010, *31*, 1–8.
[20] Isenberg, B. C., Dimilla, P. A., Walker, M., Kim, S., Wong, J. Y., Vascular smooth muscle cell durotaxis depends on substrate stiffness gradient strength. *Biophys. J.* 2009, *97*, 1313–1322.
[21] Katayama, Y., Battista, M., Kao, W. M., Hidalgo, A. et al., Signals from the sympathetic nervous system regulate hematopoietic stem cell egress from bone marrow. *Cell* 2006, *124*, 407–421.
[22] Pittenger, M. F., Martin, B. J., Mesenchymal stem cells and their potential as cardiac therapeutics. *Circ. Res.* 2004, *95*, 9–20.
[23] Rowlands, A. S., George, P. A., Cooper-White, J. J., Directing osteogenic and myogenic differentiation of MSCs: interplay of stiffness and adhesive ligand presentation. *Am. J. Physiol. Cell Physiol.* 2008, *295*, C1037–1044.
[24] Burdick, J. A., Khademhosseini, A., Langer, R., Fabrication of gradient hydrogels using a microfluidics/photopolymerization process. *Langmuir* 2004, *20*, 5153–5156.
[25] Khetan, S., Burdick, J. A., Patterning network structure to spatially control cellular remodeling and stem cell fate within 3-dimensional hydrogels. *Biomaterials* 2010, *31*, 8228–8234.
[26] Choi, Y. S., Vincent, L. G., Lee, A. R., Kretchmer, K. C. et al., The alignment and fusion assembly of adipose-derived stem cells on mechanically patterned matrices. *Biomaterials* 2012, *33*, 6943–6951.
[27] Byfield, F. J., Wen, Q., Levental, I., Nordstrom, K. et al., Absence of filamin A prevents cells from responding to stiffness gradients on gels coated with collagen but not fibronectin. *Biophys. J.* 2009, *96*, 5095–5102.
[28] Tse, J. R., Engler, A. J., Preparation of hydrogel substrates with tunable mechanical properties. *Curr. Protoc. Cell Biol.* 2010, *Chapter 10*, Unit 10 16.
[29] Kaushik, G., Zambon, A. C., Fuhrmann, A., Bernstein, S. I. et al., Measuring passive myocardial stiffness in Drosophila melanogaster to investigate diastolic dysfunction. *J. Cell. Mol. Med.* 2012, *16*, 1656–1662.
[30] Aguirre, K. M., McCormick, R. J., Schwarzbauer, J. E., Fibronectin self association is mediated by complementary sites with the amino-terminal one – third of the molecule. *J. Biol. Chem.* 1994, *269*, 27863–27868.
[31] Del Alamo, J. C., Meili, R., Alonso-Latorre, B., Rodriguez-Rodriguez, J. et al., Spatio-temporal analysis of eukaryotic cell motility by improved force cytometry. *Proc. Natl. Acad. Sci. USA* 2007, *104*, 13343–13348.
[32] Willert, C. E., Gharib, M., Digital particle image velocimetry. *Experiments in Fluids* 1991, *10*, 181–193.
[33] Alonso-Latorre, B., University of California, San Diego, United States – California 2010, p. 153.
[34] Jeon, N. L., Dertinger, S. K. W., Chiu, D. T., Choi, I. S. et al., Generation of solution and surface gradients using microfluidic systems. *Langmuir* 2000, *16*, 8311–8316.
[35] Kitamura, R., Pilon, L., Jonasz, M., Optical constants of silica glass from extreme ultraviolet to far infrared at near room temperature. *Appl. Opt.* 2007, *46*, 8118–8133.
[36] Hu, S., Ren, X., Bachman, M., Sims, C. E. et al., Surface-directed, graft polymerization within microfluidic channels. *Anal.Chem.* 2004, *76*, 1865–1870.
[37] Sunyer, R., Jin, A. J., Nossal, R., Sackett, D. L., Fabrication of hydrogels with steep stiffness gradients for studying cell mechanical response. *PLoS One* 2012, *7*, e46107.
[38] Marklein, R. A., Burdick, J. A., Spatially controlled hydrogel mechanics to modulate stem cell interactions. *Soft Matter* 2010, *6*, 136–143.
[39] Ciba Specialty Chemicals Inc. 2003, p. 8.
[40] Decker, C., Jenkins, A. D., Kinetic approach of oxygen inhibition in ultraviolet- and laser-induced polymerizations. *Macromolecules* 1985, *18*, 1241–1244.
[41] Dendukuri, D., Pregibon, D. C., Collins, J., Hatton, T. A., Doyle, P. S., Continuous-flow lithography for high-throughput microparticle synthesis. *Nat. Mater.* 2006, *5*, 365–369.
[42] Charest, J. M., Califano, J. P., Carey, S. P., Reinhart-King, C. A., Fabrication of substrates with defined mechanical properties and topographical features for the study of cell migration. *Macromol. Biosci.* 2012, *12*, 12–20.
[43] Gray, D. S., Tien, J., Chen, C. S., Repositioning of cells by mechanotaxis on surfaces with micropatterned Young's modulus. *J. Biomed. Mater. Res. A* 2003, *66*, 605–614.
[44] Jannat, Risat A., Dembo, M., Hammer, Daniel A., Traction forces of neutrophils migrating on compliant substrates. *Biophys. J.* 2011, *101*, 575–584.
[45] Alonso-Latorre, B., Meili, R., Bastounis, E., del Alamo, J. C. et al., *Engineering in Medicine and Biology Society, 2009. EMBC 2009. Annual International Conference of the IEEE* 2009, pp. 3346–3349.
[46] Huttenlocher, A., Horwitz, A. R., Integrins in cell migration. *Cold Spring Harb. Perspect. Biol.* 2011, *3*, a005074.
[47] Meili, R., Alonso-Latorre, B., del Alamo, J. C., Firtel, R. A., Lasheras, J. C., Myosin II is essential for the spatiotemporal organization of traction forces during cell motility. *Mol. Biol. Cell* 2010, *21*, 405–417.

© 2013 Wiley-VCH Verlag GmbH & Co. KGaA, Weinheim

[48] Saez, A., Buguin, A., Silberzan, P., Ladoux, B., Is the mechanical activity of epithelial cells controlled by deformations or forces? *Biophys. J.* 2005, *89*, L52–L54.
[49] Holle, A. W., Engler, A. J., More than a feeling: discovering, understanding, and influencing mechanosensing pathways. *Curr.Opin. Biotechnol.* 2011, *22*, 648–654.
[50] Vogel, V., Sheetz, M., Local force and geometry sensing regulate cell functions. *Nat. Rev. Mol. Cell Biol.* 2006, *7*, 265–275.
[51] del Rio, A., Perez-Jimenez, R., Liu, R., Roca-Cusachs, P. et al., Stretching single talin rod molecules activates vinculin binding. *Science* 2009, *323*, 638–641.
[52] Hoffman, B. D., Grashoff, C., Schwartz, M. A., Dynamic molecular processes mediate cellular mechanotransduction. *Nature* 2011, *475*, 316–323.
[53] Jiang, G., Huang, A. H., Cai, Y., Tanase, M., Sheetz, M. P., Rigidity sensing at the leading edge through αvβ3 integrins and RPTPα. *Biophys.J.* 2006, *90*, 1804–1809.
[54] Rhee, S., Jiang, H., Ho, C. H., Grinnell, F., Microtubule function in fibroblast spreading is modulated according to the tension state of cell-matrix interactions. *Proc. Natl. Acad. Sci. USA* 2007, *104*, 5425–5430.
[55] Moolenaar, W. H., Lysophosphatidic acid, a multifunctional phospholipid messenger. *J. Biol. Chem.* 1995, *270*, 12949–12952.
[56] Kolodney, M. S., Elson, E. L., Correlation of myosin light chain phosphorylation with isometric contraction of fibroblasts. *J. Biol. Chem.* 1993, *268*, 23850–23855.
[57] Zhang, Q., Checovich, W. J., Peters, D. M., Albrecht, R. M., Mosher, D. F., Modulation of cell surface fibronectin assembly sites by lysophosphatidic acid. *J. Cell Biol.* 1994, *127*, 1447–1459.
[58] Mills, G. B., Moolenaar, W. H., The emerging role of lysophosphatidic acid in cancer. *Nat. Rev. Cancer* 2003, *3*, 582–591.

© 2013 Wiley-VCH Verlag GmbH & Co. KGaA, Weinheim